J Mater Sci: Mater Electron (2017) 28:15127–15134
DOI 10.1007/s10854-017-7388-2

Structural, bandgap tuning and electrical properties of Cu doped ZnO nanoparticles synthesized by mechanical alloying

Bikram Keshari Das[1] · Tanushree Das[1] · Kajal Parashar[1] · Arun Thirumurugan[2] · S. K. S. Parashar[1]

Received: 23 May 2017 / Accepted: 19 June 2017 / Published online: 24 June 2017

Abstract Cu doped ZnO nanoparticles abbreviated as $Zn_{1-x}Cu_xO$ (x = 0, 0.01 and 0.03) were synthesized by mechanical alloying. The change in structure, morphology, band gap and dielectric properties of the synthesized nanoparticles were investigated by XRD, FE-SEM, FTIR, UV–Vis and impedance analyzer respectively. The incorporation of the dopant Cu into ZnO hexagonal wurtzite structure has been verified by X-ray diffraction (XRD) and the Cu doping on the structural bonding of ZnO has been verified by fourier transformation infrared spectra (FTIR). The XRD spectra shows that all the synthesized nanoparticles are single phase, hexagonal wurtzite structure and belong to the space group of $P6_3mc$.Crystallite size of Cu doped ZnO (15 nm) nanoparticles is smaller than pure ZnO (18 nm) and peak broadening exists in the system. FE-SEM analysis indicates that Cu doping affects the surface morphology of ZnO. The band gap (E_g) of ZnO decreases with Cu doping which can be attributed to sp-d exchange interaction between the ZnO band electrons and localized d electrons of Cu^{2+} ions. The dielectric constant of ZnO decreases with Cu doping.

1 Introduction

In semiconductor technology, the modification of ZnO properties by incorporation of dopant has become an important topic. Doping plays an important role in changing the physical properties such as electrical, optical, magmatic, piezoelectric and electronic properties of ZnO [1].The doping in ZnO provides a material with versatile characteristics makes them suitable for various device fabrication. Undoped and doped ZnO nanoparticles can be fabricated by a number of synthesis methods like, sol–gel, combustion, precipitation, solvothermal, microwave, spray pyrolysis, hydrothermal, chemical vapour deposition, mechanical alloying etc. Mechanical alloying is superior over other methods because, it reduces phase transition temperature, thermal decomposition temperature, annealing and sintering temperature, reducing phase transformation temperature, and increasing particle reactivity [2]. It also reduces particle size to the nano scale level, easily produce amorphous phase and low temperature solubility limit of doping metal can be extended [3]. Among various dopants, transition metal elements like V, Ni, Mn and Cu have been successfully employed into ZnO, because of partially filled *d* shells, which give rise to unpaired electrons [4, 5].The introduction of transition metal ions into the ZnO lattice will exhibit ferromagnetic behavior [5]. In particular, copper which has similar ionic radius to that of Zn^{2+} ion and electronic shell structure, has many physical and chemical properties similar to those of Zn [4]. From the literature, it was found that, many theoretical and experimental studies show that Cu atom is an effective dopant for ZnO. Magnetic and optical properties of Cu-doped ZnO nanosheets was investigated by Li et al. and they reported that Cu atom preferred to substitute for Zn site and induce a local magnetic moment [6]. The ZnO Bandgap can be modified by decreasing the size of the crystallites or by doping [7]. Bandgap tuning is important in material research and opto-electronic device applications. It is become important for developing highly efficient solar cells and transparent conducting oxide. It results due to the electrostatic interactions

✉ S. K. S. Parashar
sksparashar@yahoo.com

[1] Nano Sensor Lab, School of Applied Sciences, KIIT University, Bhubaneswar, Odisha 751024, India

[2] Institute of Physics, Bhubaneswar, Odisha, India

between free electrons and ionized impurities and can be compensated by Burstein–Moss effect [8, 9]. In fact doping creates distortion in the crystal lattice of pure ZnO which is related to Urbach energy [10].It explained optical transformation between occupies states valence band to unoccupied states of the conduction band. Dielectric properties (dielectric constant and dielectric loss tangent) are the most important properties of a material [11], which affect many optoelectronic and transport properties of ZnO. Therefore knowledge of dielectric constant for a material is necessary. The optoelectronic applications such as light-emitting diode (LED), UV-laser diode, photonics, nano-electronics, optoelectronics, data storage, satellite communication, EMI shielding and high speed integrated package require materials with lower dielectric constant [12]. The dielectric properties of ZnO depend on chemical composition, method of preparation, grain size and developed due to the defects of zinc excess at the interstitial position and lack of oxidation [12].The effect of temperature and frequency on the dielectric behaviour of ZnO offers various information about different polarization mechanism. Hsu and Huang have reported that, the dielectric constant of ZnO doped ($Zr_{0.98}Sn_{0.02}$) TiO4 films decreases with increase in frequency. The result was also supported by Youn et al. [13]. Das et al. studied the dielectric behaviour of Ca doped ZnO nanoceramic and reported that the dielectric constant of ZnO decreases nearly ten times with Ca doping [14].

A lot of work on ZnO and ZnO-doped materials have been published but the phenomena of change in band gap is not still understood. In the present work, we have studied extensively the structural, optical and dielectric properties of Cu doped ZnO nanoparticles synthesized by mechanical alloying.

1.1 Preparation of Cu doped ZnO nanoparticles

Stochiometry amount of ZnO (99.9%) and CuO (99.9%) powder were weighed to obtain $Zn_{1-x}Cu_xO$ where x = 0, 0.01 and 0.03 respectively. The mechanical alloying was done by a PM400Retsch, Germany High Energy Ball Milling (HEBM). Both the vessel and ball was made from tungsten carbide. The powder was milled for 10 h taking the ball to powder ratio 10:1 at 300 rpm in dry milling condition. The mixture was milled for 1 h, altering with a stop of 30 min to prevent overheating and engine wear [3]. A small amount of 3% PVA was added to the ball milled powder for the fabrication of pellet and was sintered at 1000 °C for 2 h. Both sides of the pellet were silver coated and heated at 700 °C for 15 min for dielectric measurement.

1.2 Experimental characterization

X-ray diffraction (XRD) patterns were obtained at room temperature with a PANanalytical X'Pert pro system, using Cu Kα radiation (λ = 1.54056 A°), at 45 kV and 300 mA. The surface morphological study was carried out by field emission scanning electron microscope (FESEM, Carl Zeiss NTS Ltd, UK). Absorption spectra were recorded using Lambda 750 UV/Vis/NIR Perkin Elmer spectrophotometer. The wavelength range was 300–800 nm. The fourier transformation infrared spectra (FTIR) of the prepared nanoparticles was recorded in the range of 500–4000 cm^{-1} using alpha FTIR spectrometer (Bruker). Dielectric properties was measured by using an impedance analyzer (Hioki LCR Hi-tester-3532-50) having frequencies range (100 Hz–1 MHz) and in a temperature range from (RT to 425 °C).

2 Results and discussion

2.1 X-ray diffraction studies

Figure 1a shows the XRD pattern of 10 h milled $Zn_{1-x}Cu_xO$ nanoparticles with varying concentration of Cu. The analysis of the diffraction peak shows that the crystal structure of $Zn_{1-x}Cu_xO$ nanoparticles is hexagonal wurtzite structure (space group $P6_3mc$) and well matched with JCPDS data card no. 36-1451 [14–16]. It was revealed from the XRD pattern that the peaks are along the planes (100), (002), (101), (102), (110), (103), (200), (112),(201) and (004) and the highest intensity peak is along the (101) plane. Similar peaks were reported in the literature for Cu doped ZnO [9].There is no evidence of extra peak related to Cu or any other impurities showing the synthesized nanoparticles are pure in form. This also indicates that Cu^{2+} ion successfully occupies the lattice site rather than interstitial one [1, 16] and confirm single phase formation of the sample. Compare to pure ZnO, the Cu doped sample shows lowering of intensity, broadening of peaks and it increases with increase in the concentration of Cu which is due to the reduction of crystallite size with increase in the concentration of Cu.

The variation of lattice parameter "a" and "c" with Cu concentration is shown in Fig. 1b. Generally the lattice parameters of a semiconductor depend on the external temperature, foreign atoms, strain, defects and the difference in ionic radii with respect to the substituted matrix ions [17]. From Fig. 1b, a variation of lattice parameter was observed with Cu doping. The lattice parameter "a" increases rapidly for x = 0.01 then slowly for x = 0.03. Similar variation was observed for "c" also. The change in lattice parameter is due to the difference in ionic radii of Zn^{2+} and Cu^{2+} ions. This also provides an indirect

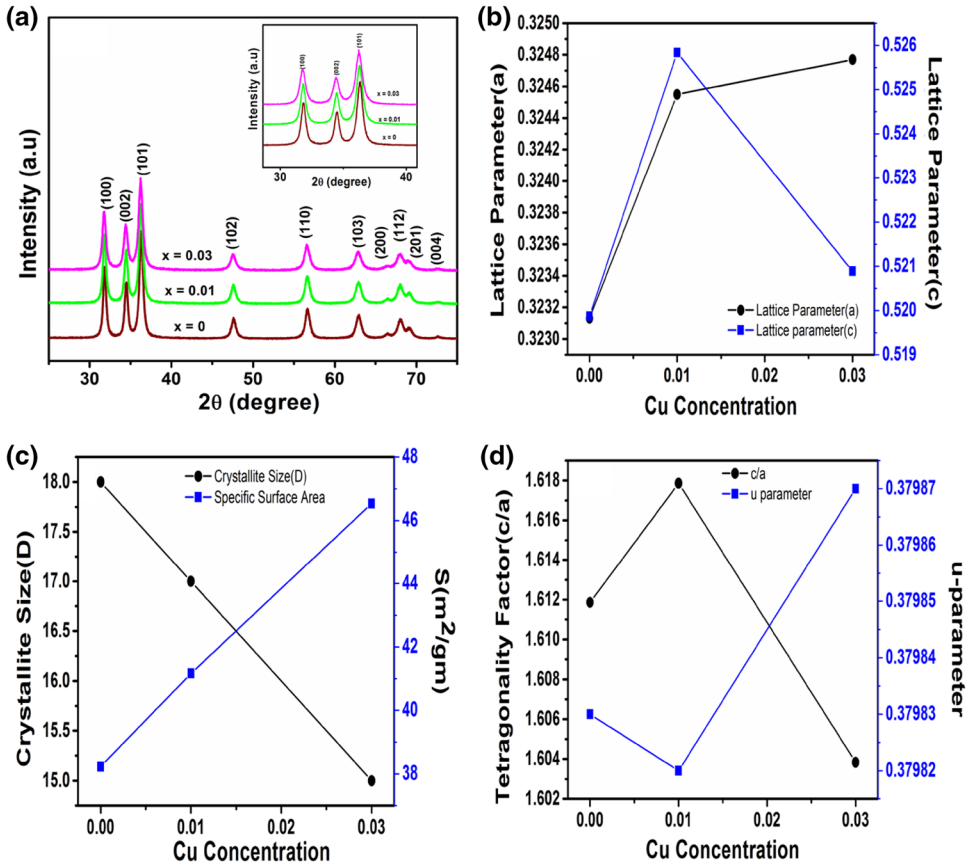

Fig. 1 **a** XRD pattern with insert zoomed in view of XRD, **b** variation of lattice parameter *a* and *c* with Cu concentration, **c** variation of crystallite size and specific surface area with Cu concentration and **d** variation of Tetragonality factor (*c*/*a*) and *u*-parameter with Cu concentration of 10 h milled $Zn_{1-x}Cu_xO$(x = 0,0.01 and 0.03) nanoparticles

evidence for the substitution of Cu^{2+} into ZnO crystal lattice following the Vegard's law [18].The variation of crystallite size (D) and specific surface area (SSA) with Cu concentration is shown in Fig. 1c. The crystallite size (D) of the synthesized nanoparticles were calculated from the broadening of the XRD reflection peaks using Debye–Scherrer's Eq. [1].

$$D = 0.9\lambda/\beta\cos\theta \tag{1}$$

The calculated crystallite size are 18, 17 and 15 nm (x = 0, 0.01, 0.03) respectively. Here reduction in crystallite size was observed which may be due to the difference in ionic radii of two ions Zn^{2+} (0.60 A°) and Cu^{2+}(0.73 A°) which causes lattice distortion [14, 19]. Another reason is that the presence of Cu^{2+} ion in ZnO prevents the growth of crystal grains. It was observed that with Cu doping the crystallite size of ZnO decreases and is monotonic with Cu concentration. Decrease in crystallite size is mainly due to the distortion created in ZnO lattice by the incorporation of impurity (Cu^{2+}) which reduces the nucleation and subsequent growth rate by the addition of Cu. The specific surface area (SSA) is a material property of solid. It measures the total surface area per unit volume. It has a particular importance in the case of adsorption, heterogeneous catalysis and reaction on surfaces [20].The specific surface area (SSA) for $Zn_{1-x}Cu_xO$ nanoparticles was calculated by using the relation [20].

$$S = \frac{6\times 10^3}{D_p \times \rho} \tag{2}$$

where S is the specific surface area, Dp is the size of the particle (nm), ρ is the density of ZnO (5.606 gm cm^{-3}) and is shown in Fig. 1c. Figure 1c clearly shows that Cu doped ZnO has a larger value of SSA than a pure one. This large value of SSA is the signature of high aspect ratio for nanostructure material and therefore enabling enhanced catalytic activity [21].

The effect of doping on bond length (L) for Zn–O is given by the relation [22]

$$L = \sqrt{\frac{a^3}{3} + \left(\frac{1}{2} - u\right)^2 c^2} \tag{3}$$

Figure 1d shows the variation of tetragonality factor (c/a) and u-parameter with Cu concentration. The oxygen positional parameter (u) was calculated for all sample by using the relation [18]

$$u = \frac{1}{3}\left(\frac{a^2}{c^2}\right) + \frac{1}{4} \tag{4}$$

Table 1 δ is the dislocation density along the plane (100), (002) and (101)

Composition	$\delta(\times 10^{15}\ m^{-2})$		
	(100)	(002)	(101)
x = 0	5.08785	4.94483	6.51147
x = 0.01	4.09788	6.11583	7.27449
x = 0.03	7.24307	8.08122	8.59223

The relative displacement between Zn & O sub lattice along the c-axis is given by u parameter and is found to increase when $\frac{c}{a}$ ratio decreases. In a wurtzite structure, the $\frac{c}{a}$ ratio deviates from the ideal value when bonding character becomes more ionic [17]. The bond length (Zn–O) given in Table 1 is found to reduce with Cu substitution for x = 0.01 and increases for x = 0.03 which cause a small structural distortion in the crystal structure [23].

The average value of dislocation density was calculated by taking first three major planes (100), (002) and (101) using the relation [24]

$$\delta = \frac{15\beta\cos\theta}{4aD} \tag{5}$$

where δ is the Dislocation density, β is the Broadening of diffraction line measured at half of its maximum intensity (radian), a is the Lattice constant(nm) and D is the Particle size(nm).

The value of dislocation density for 1st three major peaks for the plane (100), (002) and (101) was calculated and shown in Table 1. It was observed that the dislocation density value for Cu doped ZnO nanoparticles are higher and in plane (101) has highest value for all. Among all the compositions x = 0.03 shows the highest value of dislocation density indicates the highest hardness among all the compositions [25].

The schematic representation of crystalline supercell of $Zn_{1-x}Cu_xO$, which are drawn from XRD data is depicted in Fig. 2.The ideal ZnO has a hexagonal wurtzite structure. A 3 × 3 × 3 supercell of the wurtzite ZnO is shown in Fig. 2a, where the supercell contains108 atoms, specifically 54 Zn atoms and 54 O atoms. When one Zn atom is substituted by one Cu atom, it is called 1% Cu-doped ZnO (x = 0.01). Hence 1% Cu-doped ZnO supercell contains 53 Zn atoms, 1 Zn substituted Cu atom and 54 O atoms as shown in Fig. 2b. When three of Zn atom was replaced by three Cu atoms, it is called 3% Cu-doped ZnO(x = 0.03), where the supercell contains 108 atoms including 51 Zn atoms, 3 Cu atoms and 54 O atoms, is depicted in Fig. 2c.

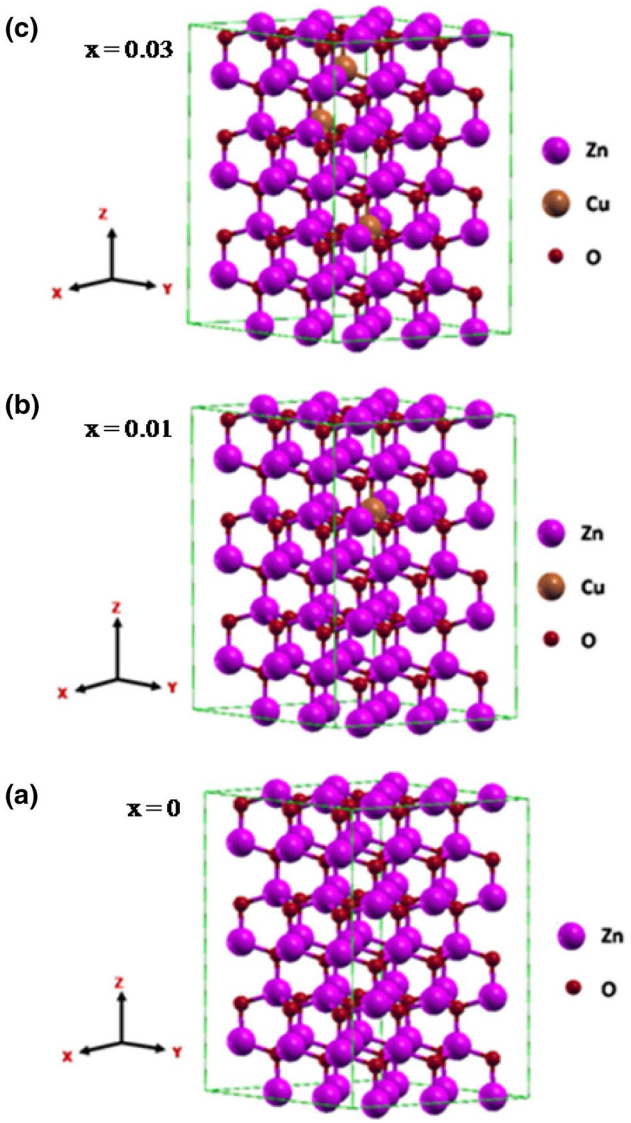

Fig. 2 Schematic representation of crystalline supercells of $Zn_{1-x}Cu_xO$ **a** x = 0, **b** x = 0.01 and **c** x = 0.03 nanoparticles

2.2 FE-SEM analysis

The surface morphology of 10 h milled $Zn_{1-x}Cu_xO$ (x = 0, 0.01 and 0.03) nanoparticles have been carried out by a field emission scanning electron microscope. The surface study provides valuable information regarding the shape and size of the particles. Figure 3(left) shows FE-SEM images of $Zn_{1-x}Cu_xO$ (x = 0, 0.01 and 0.03) nanoparticles. It clearly shows most of the particles are in spherical shape and are in the nanometric region. The individual particles agglomerate to give bigger particles of various shapes. In Fig. 3(right), it was noticed that the average particle size increases with increase in dopant concentration. The average particle size was calculated by using ImageJ software shown in Fig. 3(right) and was found to be 30, 22 and

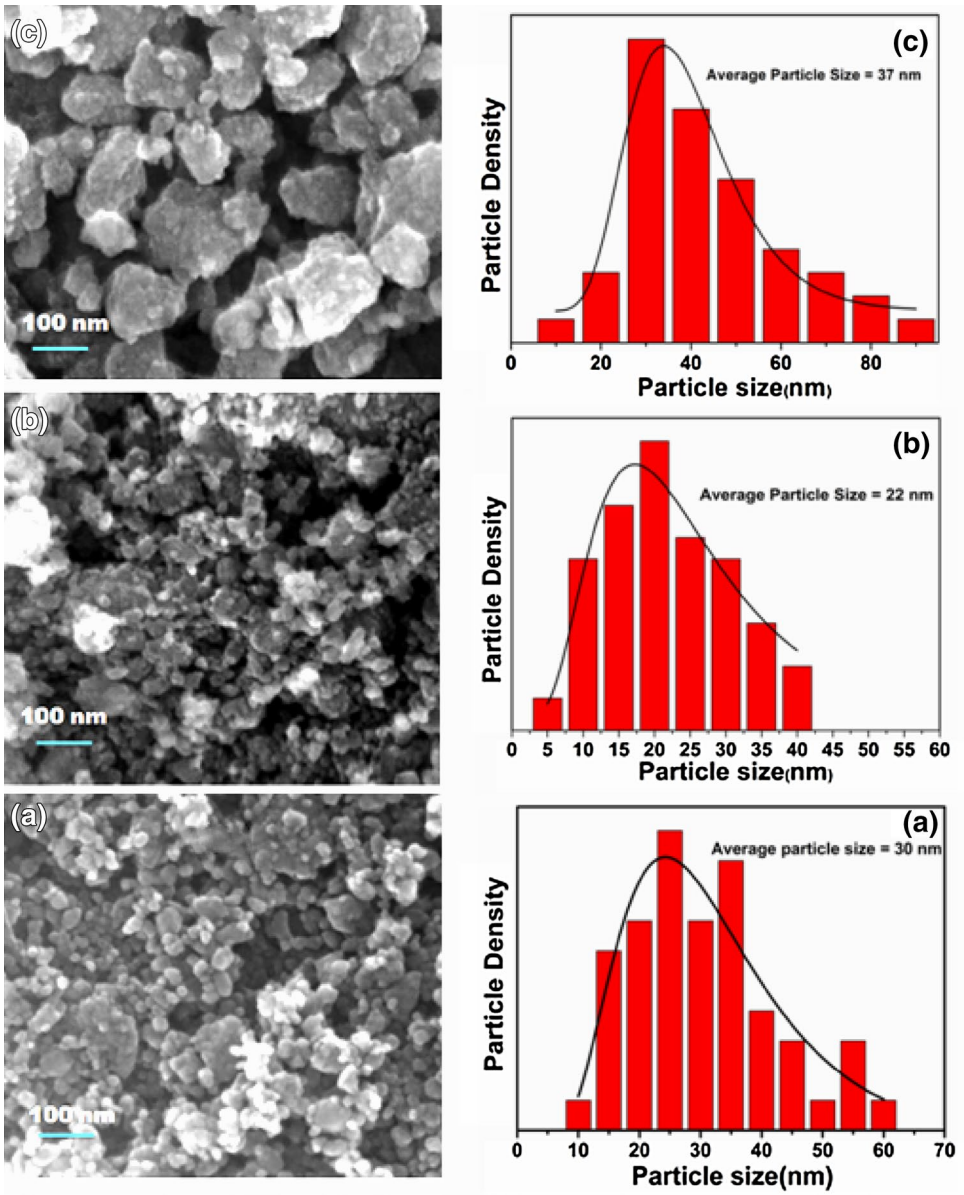

Fig. 3 (*left*) FE-SEM (*right*) particle size distribution pattern of 10 h milled $Zn_{1-x}Cu_xO$ **a** x = 0 **b** x = 0.01 and **c** x = 0.03 nanoparticles

37 nm for x = 0, 0.01 and 0.03 respectively. A similar result was found by P. K. Labhane et al. [9].

2.3 FTIR analysis

Figure 4 shows the fourier transformation infrared spectra (FTIR) of $Zn_{1-x}Cu_xO$ (x = 0, 0.01 and 0.03) nanoparticles recorded in the range of 500–4000 cm^{-1}. The band position and number of absorption peaks depends on crystallite size, chemical composition and also on morphology [26]. Here it is carried out to study the effect of Cu doping on the structural bonding of ZnO.

A broad peak due to O–H stretching vibration was found around 3400 cm^{-1} was observed for all composition, which shows the presence of water molecule absorbed on the surface of a nanocrystalline sample [27] during measurement. A peak around 1630 cm^{-1} attribute to the first overtone of the fundamental stretching mode of O–H bond [27]. A strong, sharp and intense absorption band has been observed at 1384 cm^{-1} for all the nanoparticles. The band located at 500–600 cm^{-1} can be attributed due to the Zn–O stretching mode in the ZnO lattice. As a similar type of FTIR spectra was observed for all the synthesized nanoparticles, it shows that the hexagonal wurtzite structure of ZnO remains same after Cu doping, which is supported by XRD data.

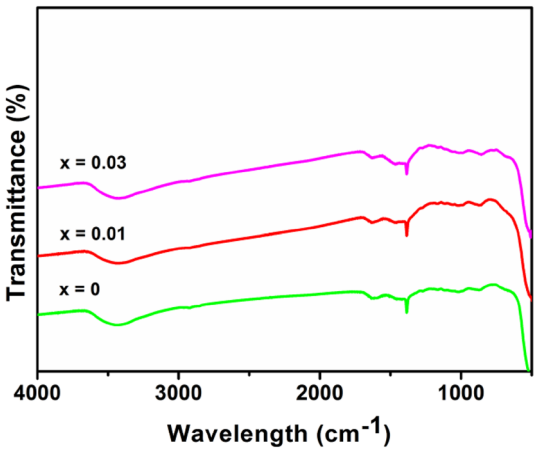

Fig. 4 FTIR spectra of 10 h milled $Zn_{1-x}Cu_xO$ (x = 0,0.01 and 0.03) nanoparticles

2.4 UV–Vis spectroscopy

Room temperature optical absorption spectra of 10 h milled $Zn_{1-x}Cu_xO$ nanoparticles has been taken in the range of 300–800 nm. All the sample showed absorption edge in the UV–Vis region and the absorption edge shows a red shift which may be due to the formation of shallow levels inside the band gap by doping [28].

The band gap energy (E_g) is an important feature of semiconductors which determine their application in opto-electronics [29]. The wide band gap of ZnO can be altered when the particles size lies in the nano region.The optical band gap of all synthesized nanoparticles was calculated by using the Tauc relation [30].

$$\alpha h\nu = A(h\nu - E_g)^n \quad (6)$$

where α is the absorption coefficient, A is a constant, h is the planck's constant, ν is the frequency of light radiation, E_g is the optical band gap energy and n = 1/2 (direct allowed transition). The band gap energy (E_g) was determined by plotting $(\alpha h\nu)^2$ versus $h\nu$ and extrapolating the linear portion of the plot to the X-axis. Figure 5 shows the variation of band gap of $Zn_{1-x}Cu_xO$ nanoparticles. It is observed that band gap decrease with increasing Cu concentration. The similar result was observed by different workers also. The observed red shift in band gap energy with an increase in Cu^{2+} concentration is due to the sp-d exchange interaction between the ZnO band electrons and localized d-electrons of Cu^{2+} ions [17]. This modification in the band gap due to Cu doping in ZnO makes them suitable for various opto-electronic and Photocatalytic applications. The variation of crystallite size and band gap with Cu concentration is shown in Fig. 5d.It was observed from Fig. 5d that both crystallite size and band gap decreases with increase in Cu concentration.

2.5 Dielectric study

Figure 6(i) shows the variation of dielectric constant (ε) as a function of temperature at 10 kHz for $Zn_{1-x}Cu_xO$ (x = 0, 0.01and 0.03). It was observed from the Fig. 6(i) that the maximum value of dielectric constant decreases with Cu^{2+}

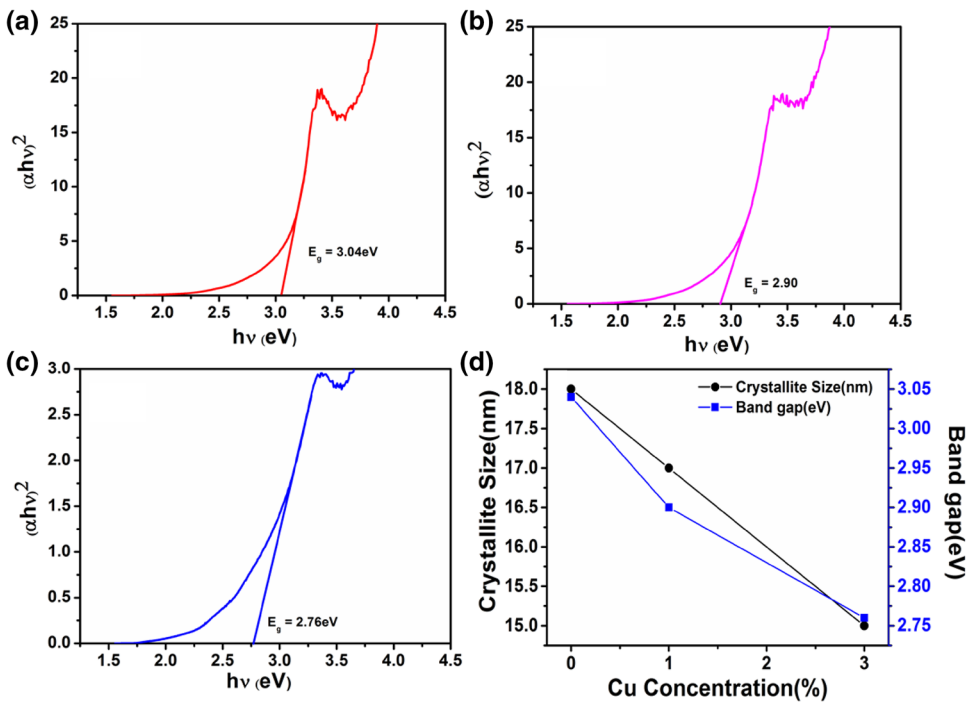

Fig. 5 Variation of band gap with Cu concentration of 10 h milled $Zn_{1-x}Cu_xO$ **a** x = 0 **b** x = 0.01 and **c** x = 0.03 nanoparticles and **d** variation of band gap and crystallite size with Cu concentration

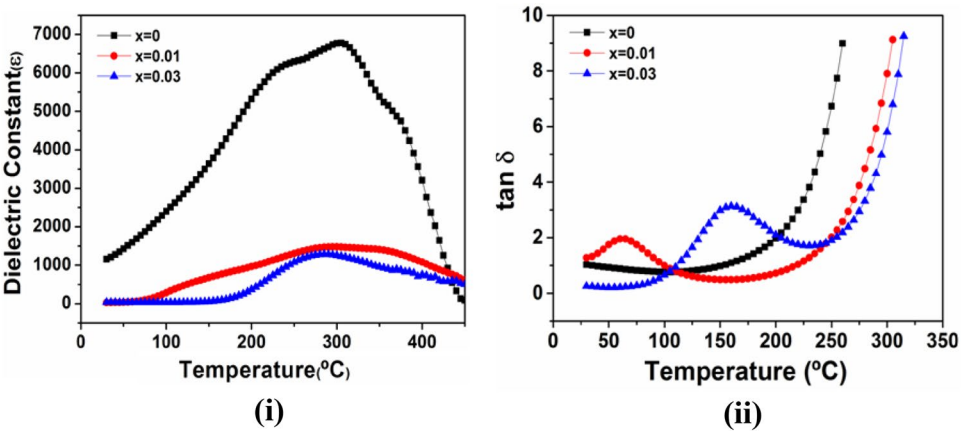

Fig. 6 **i** Variation of dielectric constant. **ii** Dielectric loss of 10 h milled $Zn_{1-x}Cu_xO$ nanoparticles at 10 kHz

doping. The decreased value of dielectric constant is due to the inhibition of dipole rotation which is caused by the substitution of the Cu^{2+} ion into ZnO. It was observed from the figure that the value of dielectric constant decreases with increase in Cu concentration. This may be due to the small dielectric polarizability of Cu^{2+} ion compared to Zn^{2+} ion. With increase in Cu doping concentration more Zn^{2+} ions will be substituted by Cu^{2+} ions resulting in the decrease of dielectric polarization. Therefore causing a decrease in dielectric constant [1].

Figure 6(ii) shows the variation of dielectric loss as a function of temperature. Generally the energy loss is expressed by dielectric loss factor (tan δ). It was calculated by domain wall resonance. The dielectric loss curve shows a linear variation for ZnO where as it shows peaking behaviour (relaxation peaks) with Cu doping at low temperature. But at higher temperature, it shows a significant increase due to space charge polarisation [1]. The appearance of relaxation peak explains the process of hopping of localised charge carriers [31]. It indicates that the hopping mechanism is operative in the system. Again this peak shifts towards higher temperature side with increase in Cu concentration. It is also found that dielectric loss increase with increase in Cu concentration.

3 Conclusions

Single phase Cu doped ZnO ($Zn_{1-x}Cu_xO$) nanoparticle has been successfully synthesized by mechanical alloying. The variation in lattice parameter, crystallite size, dislocation density, specefic surface area, bond length shows the incorporation of Cu^{2+} ion into ZnO crystal lattice causing a small structural distrotion in the structure. FE-SEM analysis shows that most of the particle are spherical in shape.The hexagonal wurtzite structure of ZnO remains unchanged after Cu doping observed from FTIR. A decrease in band gap was observed with Cu doping. Dielectric constant was found to decrease with Cu doping and peaking behaviour was observed in dielectric loss of Cu doped ZnO nanoparticles. This observation was found to be useful for various dielectic, optoelectronic and photcatalytic applications.

References

1. T. Das, B.K. Das, K. Parashar, S.K.S. Parashar, Bull. Mater. Sci. **40**, 247–251 (2017)
2. J. Wang, J.M. Xue, D.M. Wan, B.K. Gan, J. Solid State Chem. **154**, 321–328 (2000)
3. C. Suryanarayana, Prog. Mater. Sci. **46**, 1 (2011)
4. A. Mhamdi, R. Mimouni, A. Amlouk, M. Amlouk, S. Belgacem, J. Alloys Compd. **610**, 250–257 (2014)
5. N.R. Yogamalar, A.C. Bose, Prog. Nanotechnol. Nanomater. **2**, 1–20 (2013)
6. C. Xia, F. Wang, C. Hu, J. Alloys Compd. **589**, 604–608 (2014)
7. N. Kamarulzaman, M.F. Kasim, R.R. Kamarulzaman et al., Nanoscale Res. Lett. **10**, 346 (2015)
8. J.A. Sans, J.F. Sánchez-Royo, A. Segura, Superlattices Microstruct. **43** 362–367 (2008)
9. P.K. Labhane, V.R. Huse, L.B. Patle, A.L. Chaudhari, G.H. Sonawane, J. Mater. Sci. Chem. Eng. **3**, 39–51 (2015)
10. T. Larbi, B. Ouni, A. Boukachem, K. Boubaker, M. Amlouk, Mater. Sci. Semicond. Process. **22**, 50–58 (2014)
11. G. Srinet, R. Kumar, V. Sajal, Ceram. Int. **39**, 7557–7561(2013)
12. A. Franco Jrn, H.V. Pessoni, Mater. Lett. **180**, 305–308 (2016)
13. M.L. Dinesha, G.D. Prasanna, C.S. Naveen, H.S. Jayanna, Indian J. Phys. **87**, 147–153 (2013)
14. T. Das, B.K. Das, K. Parashar, S.K.S. Parashar, Acta Phys. Pol. A **130**, 1358–1362 (2016)
15. T. Das, B.K. Das, K. Parashar, S.K.S. Parashar, N.rao A, Adv. Mater. Res. **938**, 63–70 (2014)
16. S. Muthukumaran, R. Gopalkrishnan, Opt. Mater. **34**, 1946–1953 (2012)
17. U. Ozgur, Y.I. Alivov, C. Liu, A. Teke, M.A. Reshchikov, S. Dogan. J. Appl. Phys. **98**, 1–103 (2005)
18. N.-E. Sung, S.-W. Kang, H.-J. Shin, H.-K. Lee, I.-J. Lee, Thin Solid Films **547**, 285–288 (2013)
19. P.K. Sharma, R.K. Dutta, A.C. Pandey, J. Magn. Magn. Mater. **321**,4001–4005 (2009)
20. J.-Y. Park, Y.-J. Lee, K.-W. Jun, J.-O. Baeg, D.J. Yim, J. Ind. Eng. Chem. **12**, 882 (2006)
21. A. Sahai, N. Goswami, Phys. E **58**,130–137 (2014)

22. H.H. AbuulrahmanSyedahamed, C. Kartikeyan, V. Senthil, S. Kumarsan, G. Ravi, J. Mater. Chem. B **43**, 5950 (2013)
23. P. Kumar, Y. Kumar, H.K. Malik, S. Annapoorni, S. Gautam, K.H. Chae, K. Asokan, Appl. Phys. A **14**, 453–457 (2013)
24. Y.P. Venkata Subbaiah, P. Prathap, K.T. Ramakrishna Reddy, Appl. Surf. Sci. **253**, 2409 (2006)
25. R. John, R. Rajakumari, Nano Micro Lett. **4**, 65–72 (2012)
26. Z.R. Khan, M.S. Khan, M. Zulfequar, M.S. Khan, Mater. Sci. Appl. **2**, 340–345 (2011).
27. J. Singh, M.S.L. Hudson, S.K. Pandey, R.S. Tiwari, O.N. Srivastava, Int. J. Hydrog. Energy **37**, 3748–3754 (2012)
28. K.G. Saw, N.M. Aznan, F.K. Yam, S.S. Ng, S.Y. Pung, PLoS ONE **10**, 0141180 (2015)
29. M. Willander, O. Nur, Q.X. Zhao, L.L. Yang, M. Lorenz, B.Q. Cao, J.Z. Perez, C. Czekalla, G. Zimmermann et al., Nanotechnology **20**, 332001 (2009)
30. X. Linhua, S. Xiao, C. Zhang, G. Zheng, J. Su, Z.L. Wang, J. Mater. Chem. Phys. **148**, 720–726 (2014)
31. C. Jayachandraiah, G. Krishnainah, Adv. Mater. Lett. **6**, 743–748 (2015)